

MULTISCALE CHARACTERISATION OF ENVIRONMENTALLY ASSISTED CRACKING IN Al-Zn-Mg-Cu ALUMINIUM ALLOYS

*V. Landais¹, J. Robson¹, J. Carr¹ and J. Fellowes²

¹*School of Materials*

University of Manchester, UK

(*Corresponding author: virginie.landais@postgrad.manchester.ac.uk)

²*School of Earth and Environmental Sciences*

University of Manchester, UK

ABSTRACT

Aerospace Al-Zn-Mg-Cu (7xxx) alloys are known to be susceptible to environmentally assisted cracking (EAC). This phenomenon has been studied intensively for many decades, leading to empirically adopted methods to mitigate this problem through overaging and composition design. In parallel, many theories have been developed to explain EAC in 7xxx, but none is yet universally accepted. Today, a number of emerging techniques offer potential to shed new light on EAC in 7xxx. The purpose of the present paper is to demonstrate how X-ray tomography (XCT) combined with electron microscopy can be used to identify the true crack path in 3-dimensions, and hence identify material for site specific electron microscopy analysis. Composition mapping over large areas to high accuracy has been performed using a modern electron microprobe analysis system. This has been combined with transmission electron microscopy to investigate local composition in matrix and precipitates at high resolution. This combination of techniques across length scales offers the potential to provide new insights into the links between local composition, microstructure, and EAC resistance.

KEYWORDS

Environmentally assisted cracking, X-ray tomography, Electron probe microanalysis, Transmission electron microscopy

INTRODUCTION

Environmentally-assisted cracking (EAC) is a phenomenon which dramatically decreases the performance of metals and can cause premature failure of large structures. Observed in situations where components were not subjected to critical loads and no widespread corrosion was involved, this type of brittle failure is extremely difficult to predict. The EAC designation covers a number of phenomena, e.g. stress corrosion cracking (SCC), hydrogen embrittlement (HE), corrosion fatigue (CF), etc. Initially identified in steels, EAC can also affect other metals such as high-performance aerospace aluminium alloys, and this phenomenon has been a concern for industries for decades. Extensive research has been conducted on the effects of various environments (moist air, saline water, dry hydrogen gas, etc.) on microstructures and crack propagation, however no consensus has been reached and the exact nature of the mechanisms that control EAC is still being debated (Birnbaum & Sofronis, 1994; Gangloff, 2007; Holroyd & Scamans, 2013; Lynch, 2012; Oriani, 1972; Scamans, Alani & Swann, 1976, Young & Scully, 2002).

To study crack propagation, X-ray Computed Tomography (XCT) has grown increasingly popular in the recent years. 3D characterisation of a cracked specimen helps revealing important features of the microstructure which could have contributed to the propagation of the fracture, such as a specific pore, an inclusion or the very tip of the crack. These features can then be reached for further examination by other 2D imaging methods in order to better understand fracture mechanisms. In the particular case of EAC cracking, XCT is a technique which can bridge the gap between the aforementioned studies often carried out either on the macroscale (e.g. mechanical testing of specimens exposed to corrosive environment) or on the microscale (e.g. electron microscopy of fracture surfaces) (Burnett, Holroyd, Scamans, Zhou, Thompson & Withers, 2015).

The present work has been conducted at the meso- and microscales defined by Burnett, using specimens of high-strength 7xxx aluminium alloys cracked by EAC in a controlled laboratory environment. Initially, XCT was used to record and analyse in 3D the typical features of these EAC-embrittled specimens, i.e. intergranular fractures showing very little fatigue or ductility. Once the location of the crack tip was identified, the specimens were further analysed at the microscale. The presence of large precipitates along grain boundaries, as well as a large precipitate-free zone (PZF) around it, have been shown to be detrimental to the fracture properties of 7xxx aluminium alloys and likely to promote intergranular crack growth at lower loads (Ogura, Hirose & Sato, 2010; Fang, Chao & Chen, 2015). In most of these alloys, the main precipitate present along the grain boundaries is the equilibrium form of the hardening precipitate (nominally MgZn_2 η -phase), and its precipitation, coarsening, and composition is heavily influenced by the local solute content of the matrix and heat treatment (Marlaud, Deschamps, Bley, Lefebvre & Baroux, 2010).

The aim of the present work was to demonstrate how XCT can be combined with site specific electron microscopy and microprobe analysis to identify the true crack path and extract and analyse material around this path. Ultimately, this work aims to identify the role of local composition and microstructure on the susceptibility for EAC in 7xxx.

MATERIALS AND METHODS

The cracked samples provided for this study have been extracted from two different rolled plates of a high-Zn, overaged 7xxx aluminium alloy (commercial temper T7651). In this paper, the rolling direction of the plates will be referred to as the long (L) direction, the width as the long transverse direction (LT), and the thickness as the short transverse direction (ST). Small specimens containing a round notch, designed to characterise crack initiation and growth, were machined from these plates. A steel conical screw was installed in each sample to load them to 90% TYS in the ST direction, and they were subsequently exposed to water vapour in environmental cabinets (70°C, 85% RH) until EAC cracks initiated at the notch. When the cracks had propagated in the L-LT plane for ~8 mm, the samples were removed from the environmental cabinets and sent to the University of Manchester for analysis.

Low resolution XCT scanning was conducted on a Zeiss Xradia Versa 520 system, using an accelerating voltage of 80 kV and a current of 87 μ A. An overview scan of the entire crack was done with the 0.39 x macro detector with binning 2, giving an effective pixel size of 12.3 μ m. An exposure time of 4 s was used and a total of 1601 projections were taken for the scan. From this overview scan of the fracture, the approximate location of the crack tip was determined and a high resolution XCT scan was obtained at this position using the same instrument. The same voltage and current settings were used for the crack tip scan in combination with the 4 x detector and binning 1, giving an effective pixel size of 1.4 μ m. An exposure time of 25 s was used and a total of 3201 projections were taken. An identical procedure was applied to scan the second cracked sample. For both specimens, the conical screw had been left in place to ensure constant opening of the crack. Data was visualised using the software Avizo.

Elemental segregation across one of the cracked samples was studied by Electron Probe Microanalysis (EPMA). The conical screw was removed from the sample and the L-ST surface was carefully polished, with ultrasonic cleaning in ethanol between each polishing step. Measurements were acquired using a JEOL JXA-8530F FEG-EPMA equipped with 4 Wave Dispersive Spectrometers (WDS) containing TAP (Mg $K\alpha$, Si $K\alpha$) and LiFL (Cu $K\alpha$, Zn $K\alpha$, Fe $K\alpha$, Mn $K\alpha$, Ti $K\alpha$) crystals. All elements were standardised against pure metals. The focused beam was operated at 20 kV, 170 nA. A first quantitative line-scan was acquired across 5 cracks near the sample notch, using a 1 μ m step size, and a series of five line-scans was obtained near the crack tip with a 2 μ m step size. The line-scans were respectively 385 μ m and 200 μ m long. Measurements were taken for all elements, except Al which was calculated as the balance. Qualitative maps of dimension 1024 x 1024 px were also obtained from the initiation region using the same beam settings, 100 ms dwell time per pixel, and 1 μ m step size.

Specimens for electron microscopy characterisation were extracted from the same plates. SEM samples and TEM foils were prepared using standard metallographic techniques. 3 mm discs were cut out of the TEM foils and further thinned by electropolishing at 15 V in a 20% nitric acid, 80% methanol solution cooled to -35°C . High resolution SEM was conducted in a FEI Magellan field emission gun scanning electron microscope (FEGSEM) operated at 5 kV. High resolution TEM and phase identification were performed using a FEI Talos F200A microscope, equipped with the ChemiSTEM Technology (X-FEG High Brightness Source + Super-X 4 SDD Windowless EDSS Spectrometers).

RESULTS AND DISCUSSION

X-ray Computed Tomography

Figure 1 shows one of the cracked samples in the as-received condition, with the conical screw still installed. The fracture was first analysed by XCT: a 3D scan of the full length of the crack was acquired at low resolution (pixel size 12.3 μ m). A volume render of the reconstructed image extracted from this scan shows an overview of the fracture in Figure 2A. The crack has initiated slightly offset from the bottom of the notch, which is visible at the top of the image, and has propagated for \sim 8.4 mm in a flat, planar intergranular mode. However, the tip of the fracture does not appear to be a regular, continuous crack front, and some branching is apparent. To examine these features in greater detail, a second XCT scan was acquired at the crack tip. This higher resolution scan (pixel size 1.43 μ m) is shown in colour in Figure 2C, superimposed onto the original low resolution scan in grey (2B).

Both high and low resolution 3D scans are built from a series of 2D 'virtual slices', which can be examined individually. An example is given in Figure 3, where 2D slices were taken across the crack front (in the LT-ST plane of the specimen). While single 2D slices may suggest that the crack is branching and sometimes propagating on a number of distinct, parallel planes, the review of successive slices indicates that the different branches of the crack often merge, and new branches appear further away. This is illustrated in Figure 3, where different propagation planes are joining up as the crack advanced. Only by looking at the full 3D structure is it apparent that the intergranular fracture consists of a network of connected branches rather than numerous isolated small cracks. The second cracked sample was scanned using the same settings, and similar observations were made.

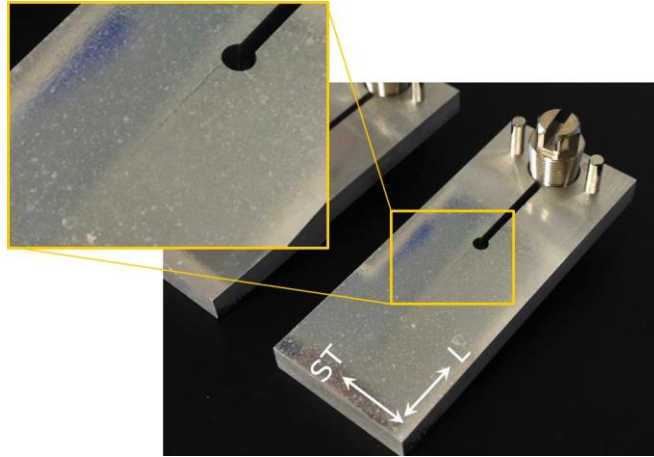


Figure 1. Typical EAC-cracked specimen in the as-received condition.

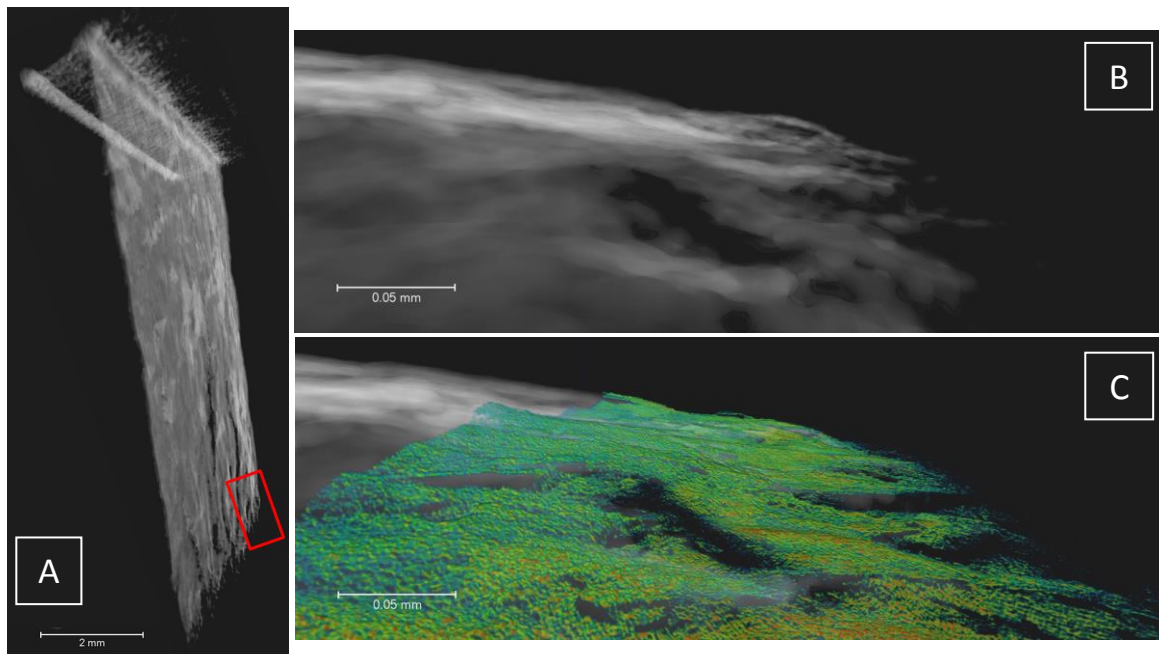


Figure 2. (A) Image extracted from the low resolution 3D XCT scan of the whole fracture. The red box indicates the location of (B) and (C). Low and high-resolution scan of the crack tip (B,C).

This non-destructive imaging technique provides a clear advantage compared to usual fracture analysis methods often used in industry, which typically involve opening the crack and examining one side of the fracture surface in a microscope. To open a crack for examination, the fracture is generally forced by static overload to break all the way through the specimen. This can damage the delicate metallic bridges created during crack branching, and can conceal the fact that the crack might have been propagating on a number of parallel planes simultaneously. Without XCT, these features would have been lost and we would only have limited evidence of how this crack initiated and propagated.

The large amount of new information brought by XCT scanning is invaluable: it allows us to identify regions of interest through the whole volume of the sample, and to select specific areas of the fracture for further examination, this time using more common “destructive” techniques.

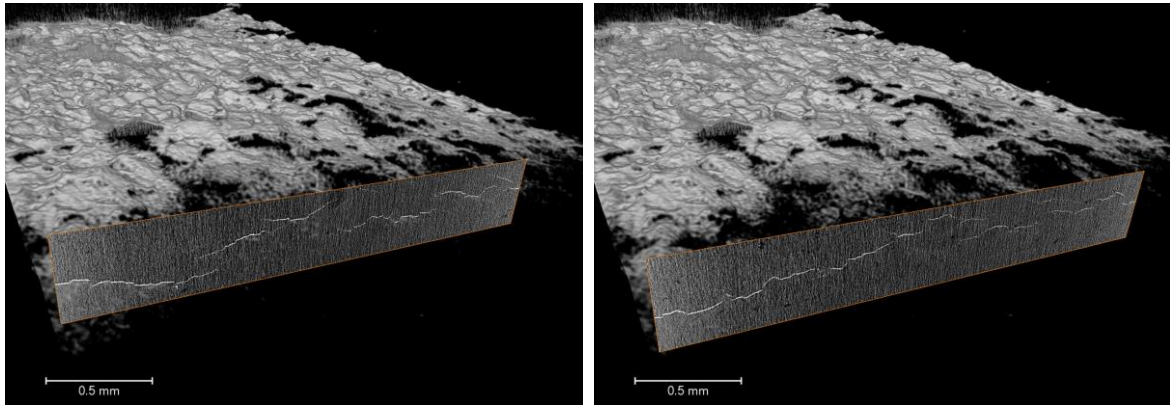


Figure 3. 2D virtual slices through the high-resolution scan of the tip, showing linking of crack branches.

Electron Probe Microanalysis

After polishing the L-ST face of one of the cracked samples, elemental analysis was conducted by EPMA. Initially, qualitative maps were obtained from the crack initiation region. The distribution of the main alloying elements Zn, Cu and Mg, is shown in Figure 4, where local variations in the concentration of all three elements are observed (see increase towards the lower right side of the maps). A more subtle variation is observed for Mg, where the concentration seems to vary from grain to grain. The Cu map shows high concentrations (in red) where coarse Cu-based precipitates such as Al_7Cu_2Fe are present, which does not allow sufficient colour contrast to observe smaller variations in the matrix like in the Mg map.

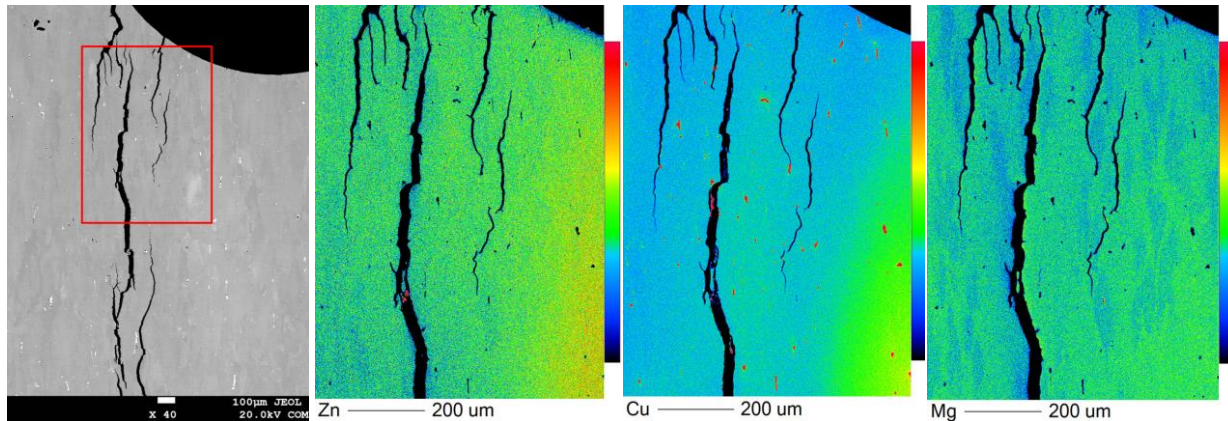


Figure 4. EPMA maps showing elemental variations of the three main alloying elements near the crack initiation region. The location of the maps is indicated by the red box in the SEM image.

To better understand the fine compositional differences in the microstructure surrounding the crack path, quantitative line-scans were acquired close to the initiation and the tip of the fracture. The red line in Figure 5B indicates the location of the first line-scan, obtained across 5 cracks near the sample notch, and the red lines in Figure 6B show the location of the scans acquired near the crack tip. The results are presented in Figures 5C-E and 6C-E. Only one of the scans near the crack tip is shown here (line 2), but the variations observed were consistent throughout the five line-scans. For all plots, the large peaks corresponding to coarse precipitates have been manually removed and a 3-point moving average trendline has been added (orange line). The error plotted for each measurement is twice the standard deviation.

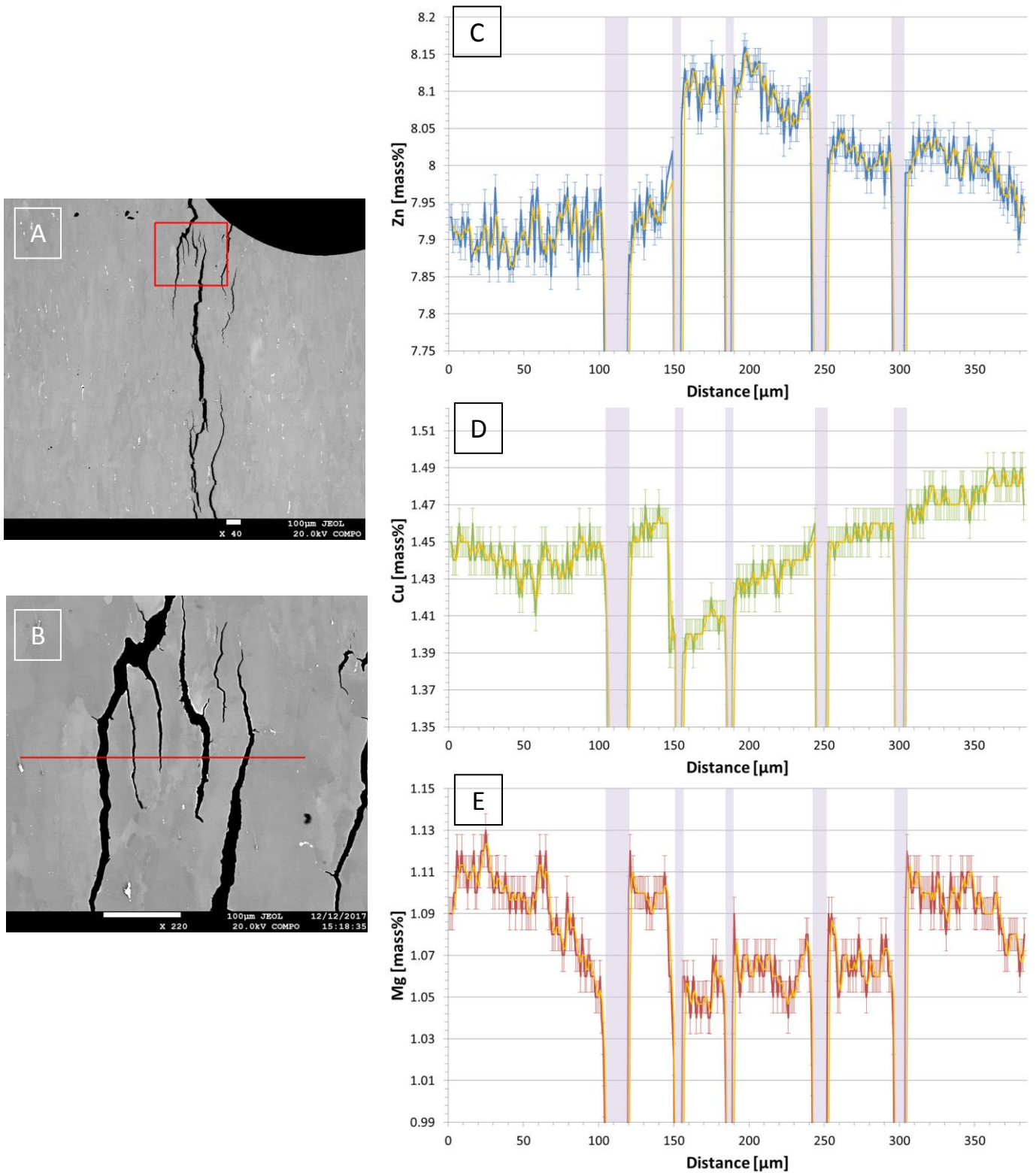


Figure 5. Quantitative line-scan showing the concentration of Zn, Cu and Mg across 5 cracks near the sample notch. The position of the scan is shown by the red line (B) and the approximate location of the cracks is indicated by the purple rectangles (C-E).

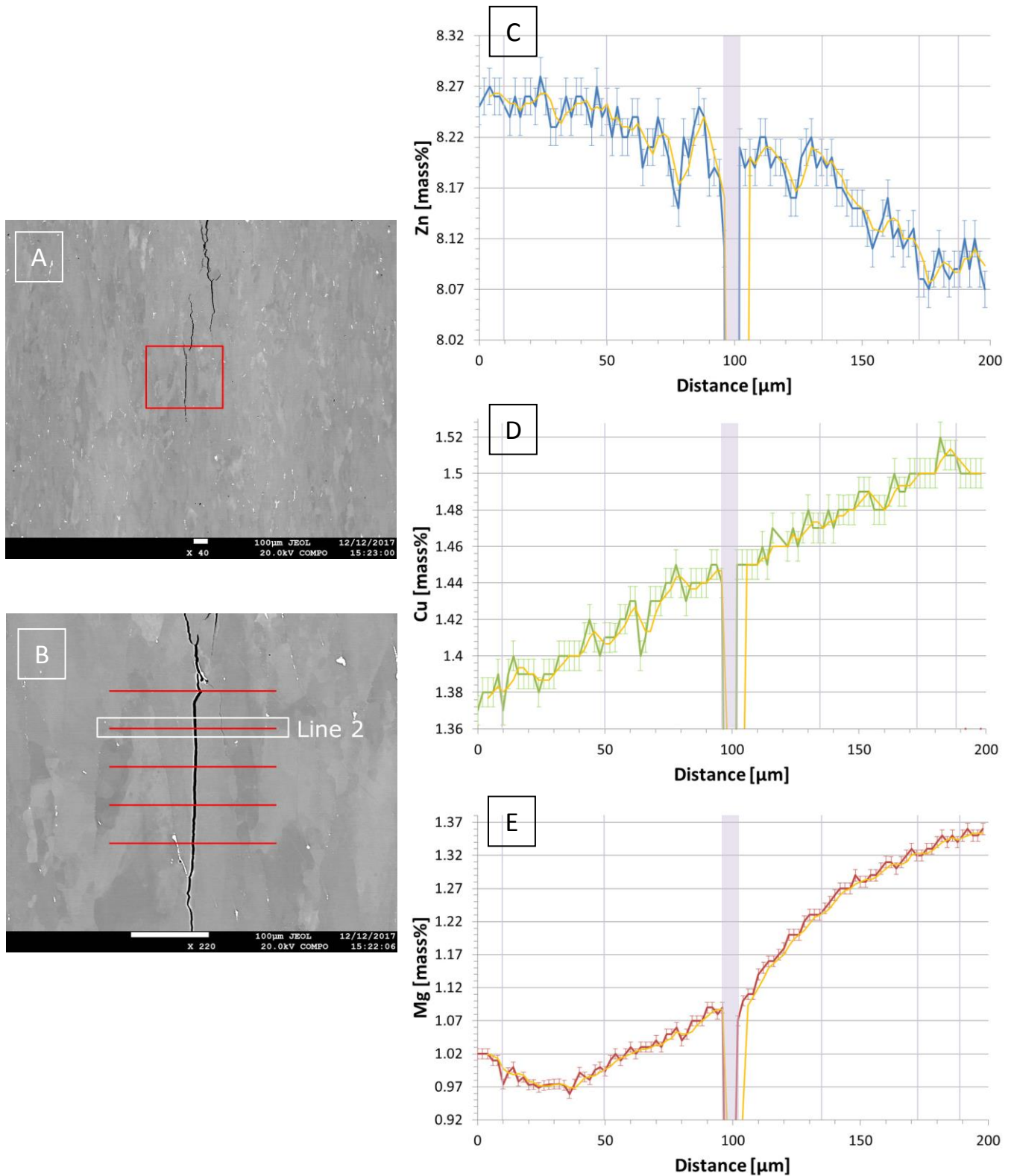


Figure 6. Quantitative line-scan showing the concentration of Zn, Cu and Mg across a crack near the tip. The position of the scan is line 2 as shown in (B). The position of the crack is indicated by the purple rectangles, and the purple lines indicate the approximate location of grain boundaries (C-E).

Across all line-scans, Zn concentration varied up to 3.7% (maximum to minimum level), Cu varied up to 9.3%, and Mg showed the largest fluctuations with a 28.7% increase. The approximate positions of the cracks along the line-scans are indicated by purple rectangles in all figures. The variations observed in Figures 6C-E near the tip do not seem to coincide with the crack path, nor with the different grains (position of the high-angle boundaries is shown by the vertical lines). Interpretation of the data collected near the initiation is less straightforward, see Figures 5C-E. Before reaching the first crack (~100 μm along the line), the scan goes across three distinct grains which show no major compositional variation. The three first cracks surround two grains (from ~120 μm to ~185 μm) that exhibit a substantial difference in composition: from left to right the Mg content decreased by 4.6%, Cu content by 4.1%, and Zn content increased by 2.6%. Variations observed across the next grains along the scan were less significant.

Overall, this EPMA analysis has highlighted the presence of notable elemental segregation. During the processing of 7xxx aluminium alloys, the rapid cooling and solidification after casting promotes the development of a dendritic structure. For micro-scale segregation, a homogenisation step is generally sufficient to allow redistribution of the solute. If this treatment was not carried out at a suitable temperature or length of time, or if the initial segregation was too severe, some compositional differences may remain (Rometsch, Zhang & Knight, 2014). Note that in places these local composition variations can exceed the composition variation permitted in the alloy specification. However, there is not a simple link between the chemical variations in the microstructure to the fracture path, which is to be expected since other factors will also contribute to the choice of crack path.

Electron Microscopy Characterisation

The importance of the grain boundary parameters (notably the PFZ dimension and the η -phase size and distribution) has been underlined in the study of intergranular EAC-cracked specimens (Ogura et al., 2010; Fang et al., 2015). So far, in this multi-scale study, each technique has provided an improved resolution and the ability to examine smaller and smaller features. In a XCT scan, features measuring at least 3 to 4 times the voxel size (pixel size³) can be resolved. The overview scan had a low resolution where only features measuring ~40 μm could be observed distinctly, but in the high-resolution scan large particles of ~5 μm in size could be detected. With EPMA, the spatial accuracy of the detection reached 1 μm . However, the resolution of these techniques is still too low to examine the grain boundaries in detail. This motivated the use of high-resolution SEM and TEM, where features on the nanometre scale can be easily imaged.

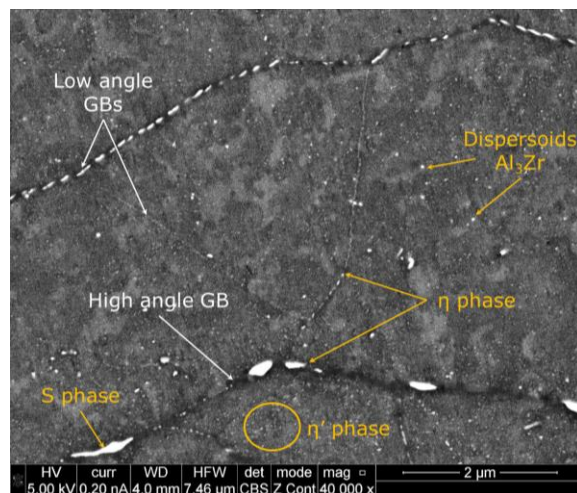


Figure 7. SEM image of the microstructure showing different grain boundaries and precipitates.

The SEM image presented in Figure 7 shows a typical subgrain of this material, where the η -phase is visible along the boundaries. A high concentration of small η -phase precipitates is found along the low angle grain boundaries delimitating the subgrains, whereas along the high angle boundaries they are noticeably larger and the spacing between them has increased. The composition of a number of grain boundary η -phase precipitates has been analysed by EDX in the TEM, see example in Figure 8. The EDX maps indicate that the η -phase has been enriched in Cu, which has been confirmed by EDX line-scans and point analysis. The Cu content of the precipitates has been previously identified as a potentially important factor in EAC, since overaging leads to an increase in Cu and (in many cases) a concomitant increase in EAC resistance. The change in composition of the η -phase will alter its electrochemical properties with respect to the surrounding matrix by making it less anodic, which could influence the EAC susceptibility of the alloy by reducing the production and uptake of hydrogen at the crack-tip (Knight, Birbilis, Muddle, Trueman & Lynch, 2010).

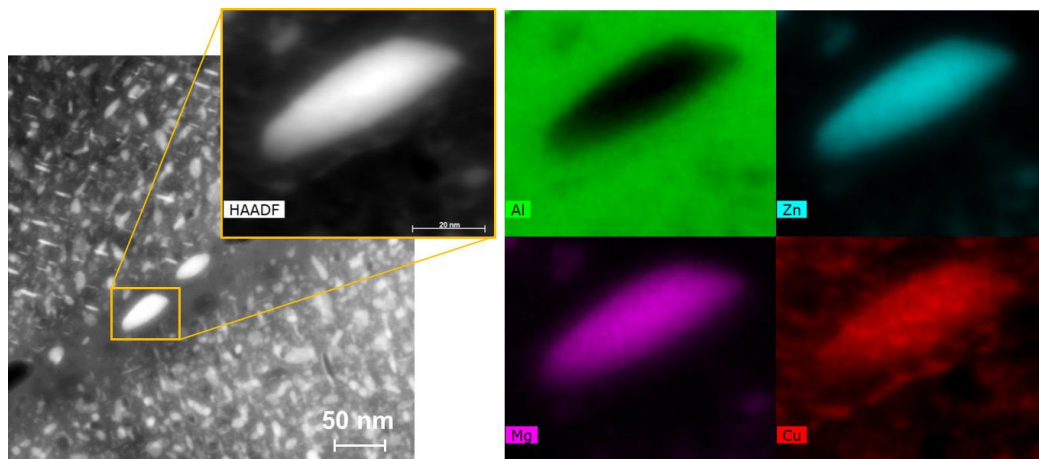


Figure 8. STEM HAADF image and EDX maps showing the composition of a grain boundary η -phase.

CONCLUSIONS

1. Examination of the EAC intergranular fractures by XCT revealed that the cracks were branching and sometimes propagating on a number of parallel planes. These branches often link up, and the overall fracture consisted of a network of connected crack branches rather than numerous isolated small cracks.
2. The presence of elemental segregation in the vicinity of the fracture was highlighted by EPMA, but there was not sufficient evidence to link these chemical variations to the fracture path.
3. EDX analysis carried out in TEM has indicated that the grain boundary η -phase MgZn_2 has been enriched in Cu.
4. The combination of multiscale characterisation methods presented in this paper permits new insights to be gained into the EAC process in 7xxx alloys. In particular, the ability to identify the true crack path by XCT, and then remove selected material around the crack for high-resolution electron microscopy, offers new opportunities to understand the link between composition, microstructure, and EAC susceptibility.

ACKNOWLEDGMENTS

We are grateful for the use of the JEOL JXA-8530F FEG-EPMA, EPSRC award EP/M028097/1, as well as for the assistance provided by the Manchester X-ray Imaging Facility, which was funded in part by the EPSRC (grants EP/F007906/1, EP/F001452/1 and EP/I02249X/1).

REFERENCES

- Birnbaum, H. K., Sofronis, P. (1994). Hydrogen-enhanced localized plasticity—a mechanism for hydrogen-related fracture. *Materials Science and Engineering A*, 176 (1–2), 191–202. [https://doi.org/10.1016/0921-5093\(94\)90975-X](https://doi.org/10.1016/0921-5093(94)90975-X)
- Burnett, T. L., Holroyd, H. N., Scamans, G. M., Zhou, X., Thompson, G. E. & Withers, P. J. (2015). The role of crack branching in stress corrosion cracking of aluminium alloys. *Corrosion Reviews*, 33 (6), 443–454. <https://doi.org/10.1515/corrrev-2015-0050>
- Fang, H.C., Chao, H. & Chen, K.H. (2015). Effect of recrystallization on intergranular fracture and corrosion of Al–Zn–Mg–Cu–Zr alloy. *Journal of Alloys and Compounds*, 622, 166–173. <https://doi.org/10.1016/j.jallcom.2014.10.044>
- Gangloff, R.P. (2007). Hydrogen-assisted cracking. In I. Milne, R. O. Ritchie, and B. Karihaloo (Ed.), *Comprehensive Structural Integrity* (pp. 301–101).
- Holroyd, H. N. J. & Scamans, G. M. (2013). Stress corrosion cracking in Al-Zn-Mg-Cu aluminum alloys in saline environments. *Metallurgical and Materials Transactions A*, 44A(3), 1230–1253. <https://doi.org/10.1007/s11661-012-1528-3>
- Knight, S.P., Birbilis, N., Muddle, B.C., Trueman, A.R. & Lynch, S.P (2010). Correlations between intergranular stress corrosion cracking, grain-boundary microchemistry, and grain-boundary electrochemistry for Al–Zn–Mg–Cu alloys. *Corrosion Science*, 52, 4073–4080. <https://doi.org/10.1016/j.corsci.2010.08.024>
- Lynch, S. P. (2012). Hydrogen embrittlement phenomena and mechanisms. *Corrosion Reviews*, 30, 105–123. <https://doi.org/10.1515/corrrev-2012-0502>
- Marlaud, T., Deschamps, A., Bley, F., Lefebvre, W. & Baroux, B. (2010). Influence of alloy composition and heat treatment on precipitate composition in Al–Zn–Mg–Cu alloys. *Acta Materialia*, 58, 248–260. <https://doi.org/10.1016/j.actamat.2009.09.003>
- Ogura, T., Hirose, A. & Sato, T. (2010). Effect of PFZ and grain boundary precipitate on mechanical properties and fracture morphologies in Al-Zn-Mg(Ag) alloys. *Materials Science Forum*, 638–642, 297–302. <https://doi.org/10.4028/www.scientific.net/MSF.638-642.297>
- Oriani, R. (1972). A mechanistic theory of hydrogen embrittlement of steels. *Physical Chemistry*, 76, 848–857. <https://doi.org/10.1002/bbpc.19720760864>
- Rometsch, P., Zhang, Y. & Knight, S. (2014). Heat treatment of 7xxx series aluminium alloys—Some recent developments. *Transactions of Nonferrous Metals Society of China*, 24(7), 2003–2017. [https://doi.org/10.1016/S1003-6326\(14\)63306-9](https://doi.org/10.1016/S1003-6326(14)63306-9)
- Scamans, G. M., Alani, R. & Swann, P. R. (1976). Pre-exposure embrittlement and stress corrosion failure in Al-Zn-Mg Alloys. *Corrosion Science*, 16, 443–459. [https://doi.org/10.1016/0010-938X\(76\)90065-2](https://doi.org/10.1016/0010-938X(76)90065-2)
- Young Jr., G. A. & Scully, J. R. (2002). The effects of test temperature, temper, and alloyed copper on the hydrogen-controlled crack growth rate of an Al-Zn-Mg-(Cu) alloy. *Metallurgical and Materials Transactions A*, 33A. <https://doi.org/10.1007/s11661-002-0009-5>